VERIFICATION OF REFINING MODELS AND THEIR APPLICATION

JAROSLAV KLOUŽEK, LUBOMÍR NĚMEC, MARCELA JEBAVÁ
MIROSLAV TROCHTA*, JIŘÍ BRADA*

Laboratory of Inorganic Materials,
Joint Workplace of the Institute of Inorganic Chemistry of the Academy of Sciences
of the Czech Republic and the Institute of Chemical Technology Prague,
Technická 5, 166 28 Prague, Czech Republic
**Glass Service, Inc., Rokytnice 60, 755 01 Vsetín, Czech Republic*

E-mail: klouzekj@vscht.cz

Submitted October 3, 2007; accepted December 14, 2007

Keywords: Glass melt, Bubble, Distribution, Models

The study compares two models of single bubble behaviour in glass melts; the steady state complete model and the simplified model utilizing the experimental data as are bubble growth rates and bubble stationary compositions. The verification of the simplified model in quiescent melt and in a real melting space shows its acceptable applicability. In addition, two models of bubble distribution in a melting space, the model of bubble representatives and the convective model, are presented. The verification procedure for both distribution models in a simple plug-flow channel indicates that the model of bubble representatives exhibits very acceptable accuracy and similar situation can be expected for more complicated melt convection. The accuracy of the convective model of bubble distribution decreases with decreasing number of classes of bubble sizes, which are used for the simulation.

INTRODUCTION

The models of bubble behaviour are rather complex and difficult for adequate mathematical description and rapid application. In addition, they need a lot of experimental data; particularly gas data in glass melts are hardly obtainable [1-3] and the values acquired by different methods have frequently only limited accuracy. That is why simplified models coming from direct observations of bubble behaviour in melts are also applied [4,5]. A verification process should nevertheless confirm their reliability. The application of simplified models plays its irreplaceable role, when formulating the particle distribution models as will be presented in the first part of this work.

Bubbles are reacting with the melt and distributed in the space by glass flow and buoyancy force. As a result of this process, the bubble concentration field evolves in the space. The high concentrations of bubbles in the melt influence the melt properties as are average melt density, viscosity and thermal conductivity, consequently the temperature and velocity fields of the melt, as well as resulting bubble concentration field. This work compares two bubble distribution models in a glass melting space:

1. The model using particle tracing (the model of bubble representatives).
2. The model based on flow of polydisperse bubble phase through the melting space (the convective model of bubble distribution).

THEORETICAL

Models of single bubble behaviour

The steady state complete model

When deriving equations governing the bubble behaviour in the melt, the universal gas equation creates the base for derivation. Thus, its form for the entire bubble is following:

$$p_t \, 4/3\pi a^3 = \sum_{i=1}^{n} \frac{m_i}{M_i} RT \tag{1}$$

and for one gas only:

$$p_i \, 4/3\pi a^3 = \frac{m_i}{M_i} RT \tag{2}$$

The total pressure, p_t, is given by:

$$p_t = p_{ex} + \rho g Z + \frac{2\delta}{a} = \sum_{i=1}^{n} p \tag{3}$$

where a is the bubble radius, g is gravity acceleration, m_i is the mass of the *i-th* gas inside the bubble and M_i is its molecular mass, R is the universal gas constant, T is absolute temperature, p_i is the partial pressure of the *i-th* gas in the bubble, p_{ex} is external pressure, Z is the depth of the bubble under melt level and δ is surface tension of the melt. After de-rivation of Equations (1) and (2) and the appropriate arrangement, the equations describing the bubble growth or dissolution, as well as its composition changes, have the form:

$$\frac{da}{d\tau}=\frac{2g^2\rho^2a^3}{27\eta\left(p_{ex}+\rho gZ+4\delta/3a\right)}+$$

$$+\frac{a\left(p_{ex}+\rho gZ+2\delta/a\right)}{3T\left(p_{ex}+\rho gZ+4\delta/3a\right)}\frac{dT}{d\tau}+ \quad (4)$$

$$+\frac{RT}{\left(p_{ex}+\rho gZ+4\delta/3a\right)}\sum_{i=1}^{n}\frac{1}{M_i}\frac{dm_i}{d\tau}$$

and:

$$\frac{dp_i}{d\tau}=\frac{3RT}{M_ia}\frac{dm_i}{d\tau}-\frac{3p_i}{a}\frac{da}{d\tau}+\frac{p_i}{T}\frac{dT}{d\tau} \quad (5)$$

In Equation (4), the Stokes´ relation for the bubble rising velocity was applied, here having the negative value with respect to the orientation of *Z*-axis:

$$\frac{dZ}{d\tau}=-\frac{2g\rho a^2}{9\eta} \quad (6)$$

where ρ and η are melt density and dynamical viscosity.

To derive the value of $dm_i/d\tau$, the Levich`s derivation was applied, relating to the mass transfer of gas between liquid and bubble of pure gas rising to the level [6]. The steady state solution of the diffusive-convective equation of gas transfer between rising bubble and melt with constant gas concentration was applied. The steady state solution assumes rapid development of gas concentration gradient around a bubble and independence of mass transfer coefficient on time. Another simplification consists in fact that the deformation of the concentration field of chemically dissolved gases around bubbles is neglected [7]. To get the value of $dm_i/d\tau$, the criterial equation may be used. The mass transfer between the bubble and melt may be described by the equation involving mass transfer coefficient, k_i [8]:

$$\frac{dm_i}{d\tau}=k_i\left(m_{ib}-m_{ia}\right) \quad (7)$$

were m_{ib} and m_{ia} are mass concentrations of the *i-th* gas in the bulk glass and on the bubble boundary, respectively.

Under conditions of constant distribution of transferred gas around the bubble (steady state), the value of k_i is given by:

$$k_i=\frac{D_iSh_i}{2a}=\frac{D_i\left[1+\left(1+Pe_i\right)^{1/3}\right]}{2a} \quad (8)$$

where D_i is diffusion coefficient, Sh_i and Pe_i are the Sherwood and Peclet numbers of the *i-th* gas, respectively. After substituting the value of Pe_i:

$$Pe_i=\frac{4a^3g\rho}{9\eta D_i} \quad (9)$$

The mass transfer coefficient of the *i-th* gas for $Pe_i >> 1$ is given by:

$$k_i=\frac{D_i}{2a}+\frac{0.382D_i^{2/3}g^{1/3}\rho^{1/3}}{\eta^{1/3}} \quad (10)$$

For growing bubbles greater then several tenths of mm, the mass transfer coefficient is considered constant with time (the first term on the right side of Equation (10) is neglected) and the Levich's solution is acquired [4]. After substituting (10) and (7) into Equations (4-5), the set of equations describing bubble behaviour is obtained.

Equations (3), (4-5) and (6) are then numerically solved to get unknown time development of a, p_i and Z. The application of the bubble model needs proper values of particularly quantities characterizing gases, namely their diffusion coefficients, solubilities and bulk concentrations (taking into account also chemical solubility of some gases). The values are acquired by laboratory measurements using different laboratory methods as are high temperature extraction of gases from the melt and their subsequent determination by gas chromatography, different methods of gas diffusivity measurements and measurements of chemical equilibria of gases in melt [1-3].

The simplified model

Any multi-component bubble in a liquid reaches after a sufficiently long time the composition which is independent from bubble initial composition and under given temperature and pressure depends only on concentration of gases dissolved in the melt [9]. Thus, if the gas distribution in the melt is homogeneous, all bubbles reach after some time identical composition, almost constant with time (slight changes of composition are brought about by changing hydrostatic pressure). Figure 1 presents schematically the developments of bubble

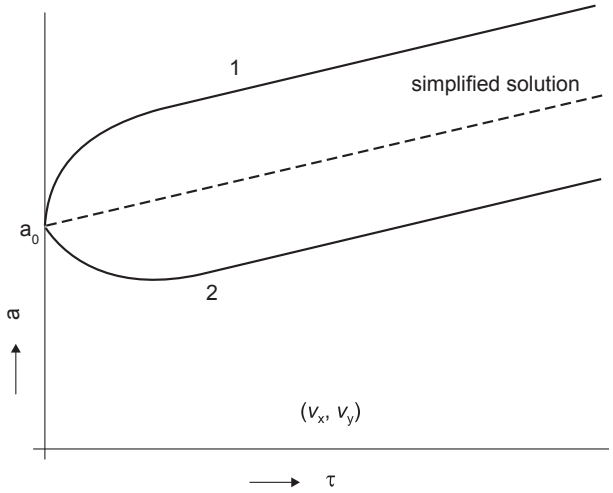

Figure 1. Bubble radius vs. time for different initial bubble compositions at constant temperature and pressure: --- bubble has the stationary composition; 1 - initial bubble contains low concentration of the decisive gas; 2 - initial bubble contains high concentration of the decisive gas (the decisive gas principally influences the bubble behaviour; mostly fining gas).

compositions to the stationary value (determined by temperature, pressure, gas concentrations and their so-lubilities in the melt), valid for different initial bubble compositions. The time necessary for a bubble to attain the stationary composition increases linearly with bubble radius, decreases approximately exponentially with sinking temperature and decreases as the initial bubble composition approaches the stationary one [9].

As the behaviour of stationary bubbles is simple (almost linear growth of bubble size with time and constant composition at constant temperature and pressure) and equivalent for all bubbles, the idea offers to replace the modelling of actual bubbles by modelling of stationary ones. The only necessary value, i.e. the bubble growth rate under stationary conditions, is measurable relatively easily by using the high temperature observation of bubble behaviour [1].

At constant temperature and under atmospheric pressure, Equation (4) may be replaced by:

$$\left(\frac{da}{d\tau}\right)_D = \Delta a/\Delta\tau \tag{11}$$

where $\Delta a/\Delta\tau$ is the bubble growth rate of stationary bubbles by the diffusion (the third term on the right side of Equation (4)), measurable in laboratory.

Under non-isothermal conditions, however, the composition of bubbles changes, which fact brings about corresponding changes of bubble sizes. Among present gases, especially chemically dissolved gases, characterized by steep temperature dependence of their solubility in melt, exhibit this effect. In a simplified case, all present gases may be classified into two groups: refining gas - whose concentration in both glass and bubbles substantially changes with temperature and other present gases - whose amount in bubbles remains almost constant as temperature varies. Taking into account this assumption, the change of bubble size due to temperature change (accompanied by the change of concentration of refining gas in the bubble) is given by [10]:

$$\left(\frac{da}{d\tau}\right)_T = \frac{a}{300-3C}\frac{dC}{d\tau} \tag{12}$$

where C is the stationary concentration of the refining gas in the bubble in volume percents.

Under non-isothermal conditions of bubble moving through the melting space, we have for $dC/d\tau$:

$$\frac{dC}{d\tau} = \frac{dC}{dT}\left[\frac{\partial T}{\partial x}v_x + \frac{\partial T}{\partial y}v_y + \frac{\partial T}{\partial z}\left(v_z - \frac{2g\rho a^2}{9\eta}\right)\right] \tag{13}$$

where v_x, v_y, v_z are the velocity components of the melt.

The value of dC/dT may be obtained from the experimentally measured dependence $C = C(T)$. The high temperature observation of shrinking bubbles under conditions of dropping temperature is used to get $C = C(T)$. Notice that $(da/d\tau)_T$ is negative when decreasing temperature.

To describe behaviour of stationary bubbles at constant glass composition and pressure, additivity of both contributions to the change of bubble size is assumed, therefore:

$$\frac{da}{d\tau} = \left(\frac{da}{d\tau}\right)_D + \frac{a}{300-3C}\frac{dC}{d\tau} \tag{14}$$

Models of bubble distribution in a melting space

Model of bubble representatives

When applying the tracing model for bubbles, the bubble trajectories are followed in a melting space. Instead of following all entering bubbles, only s.c. bubble representatives are traced [11,12]. It is assumed that the trajectory of given bubble representative differs only slightly from trajectories of represented bubbles with similar size and starting position. Consequently, the represented bubbles find their time positions on the trajectory of the bubble representative. Thus, several thousands up to tens of thousands of representative bubbles are followed instead of all inputting bubbles. When the steady state sets up, all bubbles are located on trajectories of bubble representatives and the appropriate bubble concentration field is obtained by summation of represented bubbles in appropriate elementary volumes of melt. The amount of represented bubbles on arbitrary trajectory of the bubble representative is characterized by the input frequency f_i of represented bubbles, i.e. is determined by the number of bubbles of the given class of sizes released from the elementary input surface (or input volume when nucleated bubbles are followed) and by melting performance of the space.

As is obvious, several sources of bubbles may be thus modelled; kinetics of bubble behaviour should be taken into account by applying the complete or the simplified bubble models of single bubble behaviour. Figure 2 presents the schematic trajectory of a representative bubble with positions of represented bubbles.

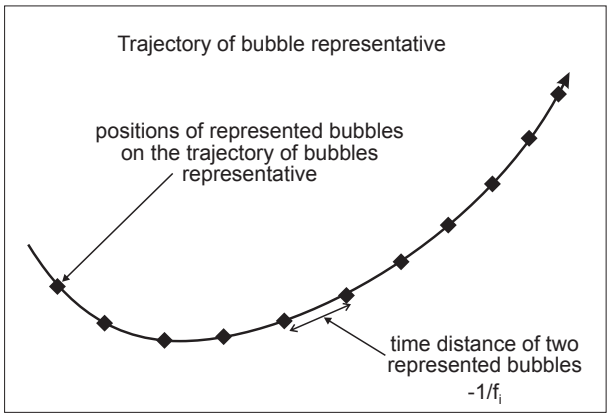

Figure 2. The schematic trajectory of bubble representative with positions of represented bubbles; f_i - the frequency of bubble input for bubbles of the *i-th* class of bubble sizes.

The convective model of bubble distribution

In the model, bubbles input the melting space as a separate phase; they are distributed by glass convection and by their own rising. The concentration of particles is further determined by their interaction with the melt, i.e. by their growth or shrinkage. The transport of bubbles by diffusion is neglected. The governing equation valid for mass concentration of monodisperse bubbles in given point of the space has the form:

$$\frac{\partial c}{\partial \tau} = -\left[v_x \frac{\partial c}{\partial x} + v_y \frac{\partial c}{\partial y} + \left(v_z - \frac{2g\rho a^2}{9\eta} \right) \frac{\partial c}{\partial z} \right] + R \qquad (15)$$

Where R is the bubble concentration change caused by their dissolution or growth:

$$R = 4\pi N_B \rho_{bub} a^2(\tau) \left(\frac{da}{d\tau} \right) = \frac{3c_{in}}{a_0^3} a^2(\tau) \left(\frac{da}{d\tau} \right) \qquad (16)$$

Here $(da/d\tau)$ is the bubble growth or dissolution rate obtainable from the simplified model of single bubble behaviour (Equation (14)), N_B is the bubble number density in the given point, ρ_{bub} is the bubble density and c_{in} is the initial mass concentration of bubbles. During numerical solution of Equations (15-16), the bubble redistribution into classes of bubble sizes is performed after each calculation step [13].

The analytical model of bubble distribution in a channel with plug flow

If polydisperze particles input the channel with plug flow, their mass concentration in the given point characterized by coordinates x and z is given by:

$$c(x,z) = c_{in} \sum_{i(a_{o\min})}^{i(a_{o\max})} \frac{f(\bar{a}_i)}{\bar{a}_{oi}^3} \bar{a}_i^3 \Delta a \qquad (17)$$

where c_{in} is the total mass concentration of particles inputting the space, $f(\bar{a}_i)$ is the probability density function of bubble size distribution for the *i-th* class of bubble sizēs, a_i is the average bubble radius in the *i-th* class of bubble sizes and in point [x,z], a_{oi} is its input radius, Δa is the width of one class of bubble sizēs and $i(a_{o\min})$, as well as $i(a_{o\max})$ designate indexes of minimum and maximum bubbles crossing the given point [x,z].

If only bubble numbers in given point are followed:

$$N(x,z) = N_{in} \sum_{i(\bar{a}_{o\min})}^{i(\bar{a}_{o\max})} f(\bar{a}_i) \Delta a \qquad (18)$$

In Equations (17-18), the constant input form of the function $f(\bar{a}_i)$ is preserved.

For particles of the same density as melt, the values of $\bar{a}_{o\min}$ and $\bar{a}_{o\max}$ merge with size classes of minimum and maximum inputting particles; however, only a part of particles may cross the given point if particles rise or fall. If bubbles are considered, the starting points of classes of bubble sizes crossing the given point [x,z] in the channel may be obtained by calculating their trajectories. The starting height z_o (x_o = 0) of a growing bubble is calculated according to the equation:

$$z_{oi} = z - \frac{2g\Delta\rho}{9\eta} \left(\bar{a}_{oi}^2 \tau + \bar{a}_{oi} \dot{a} \tau^2 + \frac{\dot{a}^2 \tau^3}{3} \right) \qquad (19)$$

where $\tau = x/v_{glass}$ and v_{glass} is the glass velocity through the channel.

If $z_o \in \langle 0;H \rangle$, where H is the height of glass layer in the channel, the given class of bubble sizes crosses the point [x,y] and bubbles of this class contribute to the total bubble concentration in the point. The total bubble concentration in the point [x,y] (expressed by Equation (17) or (18)) is the sum of all classes of bubble sizes matching up the mentioned condition.

RESULTS AND DISCUSSION

Single bubbles in a quiescent melt

The verification of applicability of the simplified model defined by Equation (12) asks for the comparison of calculated results with those coming from the complete model (Equations (4-6)). The original properties of engaged gases, i.e. their diffusion coefficients, solubilities and actual concentrations in the melt were obtained for TV glass [14]. Following examples of bubble behaviour in a quiescent melt were studied to compare both models of single bubble behaviour:

1. Behaviour of initially air bubbles and melting bubbles (95 vol.% CO_2, 5 vol.% N_2) at constant temperatures 1200-1500°C.
2. Behaviour of bubbles having stationary composition at linearly increasing or decreasing temperature.

When examining applicability of the simplified model at constant temperature, the initial bubble compositions of real bubbles coming from the massive bubble sources should be considered. The majority of mel-ting bubbles at lower temperatures contains mainly CO_2 with low amount of nitrogen while bubbles coming from refractory materials are air bubbles or bubbles containing also some CO_2 [14]. According to Figures 3 and 4, only small differences were found in behaviour of initially air bubbles when applying complete and simplified models (for the simplified model, the slope $da/d\tau$ from the stationary period of the complete model should be inserted). The slight decrease in the bubble diameter for the greater bubble, caused by oxygen absorption from the bubble into melt, gives the evidence about differences between both solutions at lower temperatures. The differences due to this effect are negligible at higher temperatures as demonstrates Figure 4.

When applying bubbles with low initial concentrations of refining gas, the differences between two models are obvious at higher temperatures as the bubbles have to reach the stationary composition characterized by high concentration of refining gas (oxygen) according to the complete model. This behaviour is obvious both from Figure 4 and Figure 5. The effect of decreasing hydrostatic pressure in the later period is obvious from the curves of the complete model.

Figure 6 providing typical results of bubble behaviour at increasing temperature shows as well the acceptable coincidence of both models. The bubbles of the initial stationary composition were elected for the comparison as the composition of freely ascending bubbles under real non-isothermal conditions is close to the stationary one. The difference between both solutions comes from the fact that the complete model reaches the stationary composition with definite rate, depending on the rate of temperature change, while the simplified model deals only with stationary bubbles. One can nevertheless conclude from the Figure 6 that bubbles at melting conditions reach the stationary composition relatively fast at growing temperature and the simplified model may be applied without great error.

When calculating behaviour of bubbles having stationary concentration of the refining gas at decreasing temperature, the bubbles described by the complete model exhibit higher inertia in growing, particularly at higher initial temperatures and higher rates of temperature decrease. This is obvious from Figure 7. If bubbles are circulating between upper and bottom layers of glass having different temperatures in the melting space, the mentioned differences may grow enough to devaluate results according to the simplified model.

The difference between the simplified and complete models could be evaluated by the comparison of bubble pathways in a real glass melting space. The initial composition of bubbles should be elected with respect to real melting conditions. Consequently, the typical composition of a melting bubble involved the

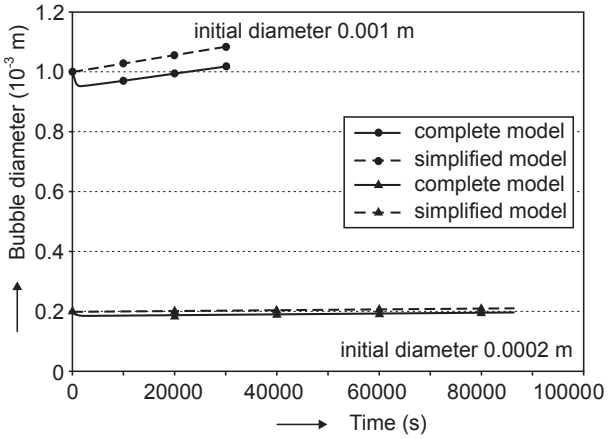

Figure 3. Behaviour of air bubbles at 1200°C calculated by the complete and simplified models.

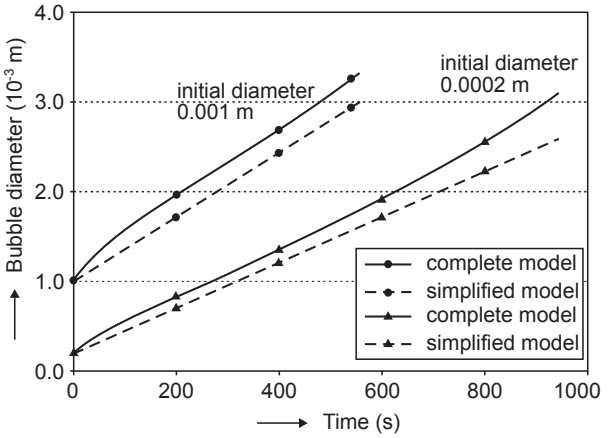

Figure 4. Behaviour of air bubbles at 1500°C calculated by the complete and simplified models.

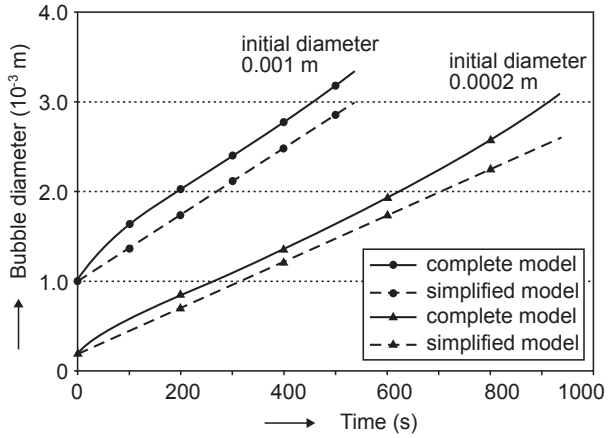

Figure 5. Behaviour of bubbles having the initial composition 95 CO_2, 5 N_2 (vol.%) at 1500°C calculated by the complete and simplified models.

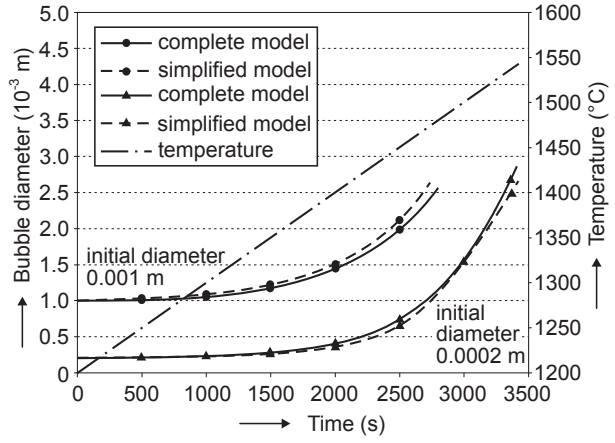

Figure 6. Behaviour of bubbles having stationary composition (15 CO_2, 85 N_2 (vol.%)) at temperature increasing from 1200°C by the rate 0.1°C/s calculated by the complete and simplified models.

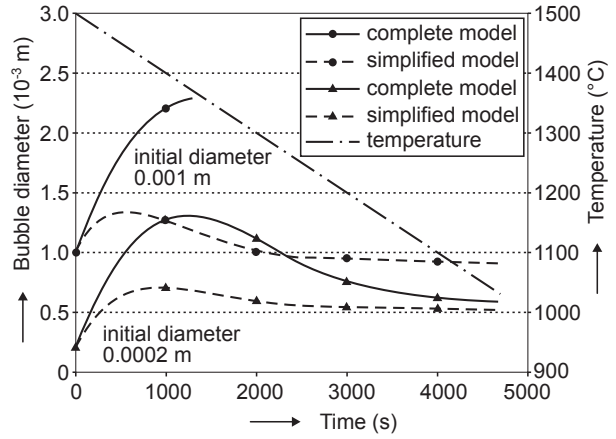

Figure 7. Behaviour of bubbles having stationary composition (1.5 CO_2, 1.0 N_2, 7.0 H_2O, 90.5 O_2 (vol.%)) at temperature decreasing from 1500°C by the rate 0.1 °C/s calculated by the complete and simplified models.

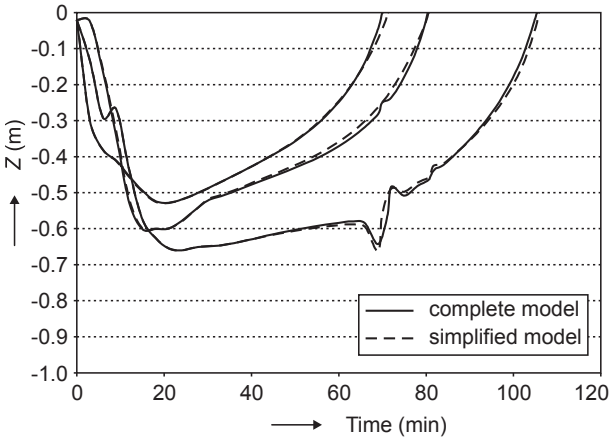

Figure 8. The pathways of bubbles from the batch (60 CO_2, 26 O_2, 9 N_2, 5 H_2O (vol.%)) in a model melting space.

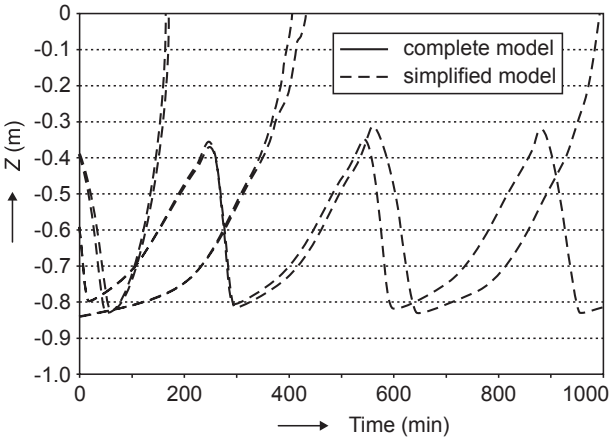

Figure 9. The pathways of air bubbles in a model melting space.

stationary concentrations of O_2 and H_2O at 1300°C; the remaining gases, CO_2 and N_2, were in the concentration ratio 7:1. In Figure 8, three melting bubbles were modelled in a melting space starting from positions below batch blanket. Figure 8 presents projections of bubble pathways into Z coordinate as a function of time according to complete and simplified solutions. As can be seen, bubbles simulated by means of both models followed almost the same histories.

The histories of air bubbles acquired by means of both models were simulated, see Figure 9. The starting points at different temperatures, ranging between 1200 and 1400°C, were elected on the boundaries between refractory materials and glass. Figure 9 demonstrates in form of $Z(\tau)$ dependence three examples of bubbles coming from furnace bottom and sidewalls. Calculated histories exhibited again an acceptable similarity despite of the fact that both temperature decrease and increase occurred along bubble trajectories. The presented results demonstrate the applicability of the simplified model under real conditions of glass melting.

Verification of bubble distribution models in the plug flow channel

Both numerical particle distribution models presented in previous paragraphs use simplifications. Their reliability for modelling studies of the refining process should be therefore verified. The usual way of verification is comparison between results of both numerical models applied under conditions of plug flow channel [15] and results of the analytical model described previously. In the following verification procedure, the concentrations and average concentrations in vertical sections through the channel obtained by the model of bubble representatives (TRACE), or the bubble convective model (PACO), are presented and compared with results from the analytical model.

A channel having length 10 m, width 4 m and depth (layer of glass melt) 1 m was chosen for verification; the melt was TV glass at 1200°C. The constant melt velocity in the longitudinal (X) direction was 0.1 mm/s. Bubbles distributed in five classes of bubble sizes were elected for verification; they entered the channel by the entire left front side. Table 1 brings the bubble size distribution and other initial conditions for entering bubbles, i.e. the initial bubble number densities in PACO model and the period of bubble inputting the surface unit in TRACE model.

Figure 10 presents the bubble number density distribution in the channel for five classes of bubble diameters with diameter growth rate 1×10^{-7} m/s when using the TRACE model. Its coincidence with the analytical plug flow model proving the correctness of the TRACE model is confirmed by Figure 11.

Table 1. The initial bubble size distributions and concentrations for distribution models.

PACO model			TRACE model		
class	d_{0i} (m)	N_{0i} (m^{-3})	class	d_{0i} (m)	$1/f_i$ (sm^2)
1	1.00×10^{-4}	1.00×10^{8}	1	1.00×10^{-4}	1.00×10^{-4}
2	2.00×10^{-4}	1.00×10^{8}	2	2.00×10^{-4}	1.00×10^{-4}
3	3.00×10^{-4}	1.00×10^{8}	3	3.00×10^{-4}	1.00×10^{-4}
4	4.00×10^{-4}	1.00×10^{8}	4	4.00×10^{-4}	1.00×10^{-4}
5	5.00×10^{-4}	1.00×10^{8}	5	5.00×10^{-4}	1.00×10^{-4}
N_{tot} (m^{-3})		5.00×10^{8}	N_{tot} (m^{-3})		5.00×10^{8}
$dd/d\tau$ (m/s)		1.00×10^{-7}	$dd/d\tau$ (m/s)		1.00×10^{-7}

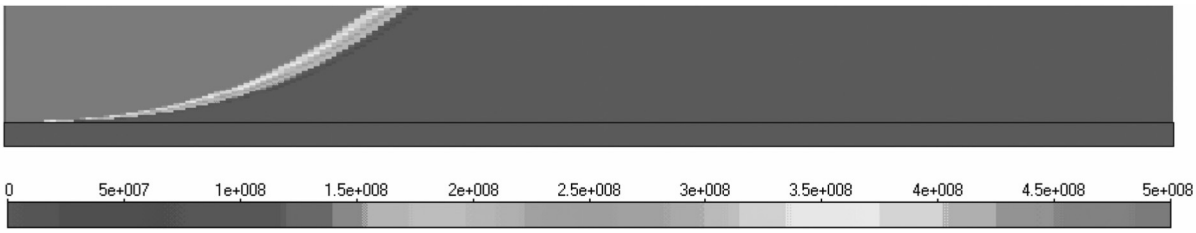

Figure 10. The bubble number density distribution in the plug flow channel. Initial conditions are in Table 1. Application of the TRACE model.

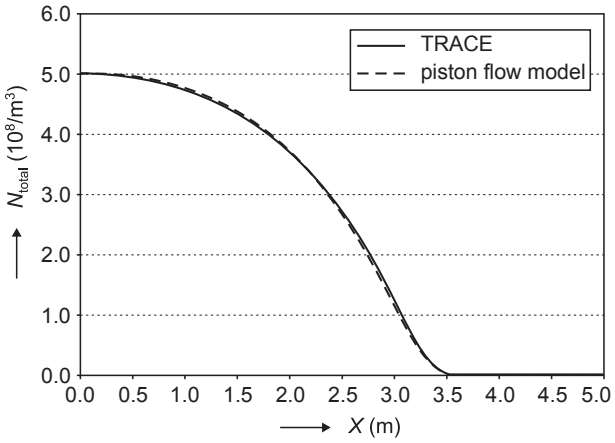

Figure 11. The average bubble number densities in vertical sections as a function of X-coordinate. The bubble distribution comes from Figure 10. The comparison of the analytical Plug flow model and the TRACE model.

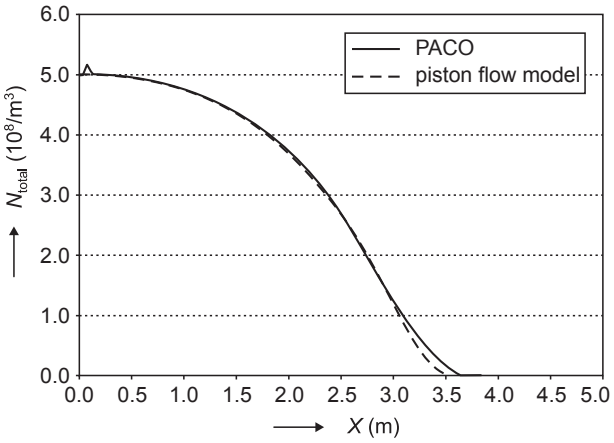

Figure 13. The average bubble number densities in vertical sections as a function of X-coordinate. The bubble distribution comes from Figure 12. The comparison of the PACO model with the analytical Plug flow model.

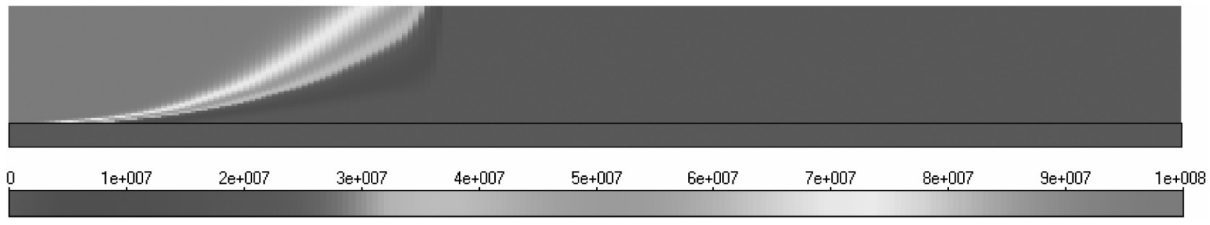

Figure 12. The bubble number density distribution in the plug flow channel. Initial conditions are in Table 1. PACO model.

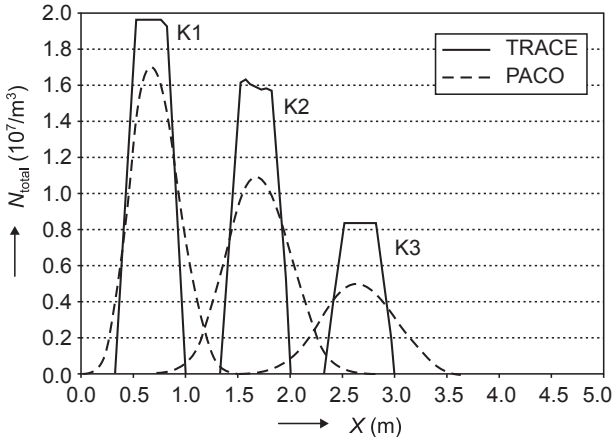

Figure 14. The areas of existence of bubbles having following sizes: K1: 0.9-1.1 mm, K2: 1.9-2.1 mm, K3: 2.9-3.1 mm. 100 classes of bubble sizes was used for the calculation.

The bubble distribution calculated by the PACO model is affected by numerical errors called "numerical diffusion". Errors arise during bubble distribution into control (elementary) volumes and during bubble redistribution into different classes of bubble sizes. Although this phenomenon was partially suppressed, the numerical diffusion still plays a role. This is apparent from Figure 12, where the same input data as in Figures 10 and 11 are used. Nevertheless, the average bubble number densities in vertical cross sections are in an acceptable consent with the plug flow model as presents Figure 13.

The "numerical diffusion" of the PACO model influences more significantly the local bubble distribution in the plug flow channel. This can be shown by the comparison between TRACE model (the bubble distribution corresponds excellently to the reference plug flow model) and PACO model, presented in Figure 14. The comparison provides areas of existence of bubbles of given sizes in the plug flow channel. The following areas of bubble sizes were calculated in the cross sections of the channel and plotted in Figure 14 as a function of channel length; K1: d = 0.9-1.1 mm, K2: d = 1.9-2.1 mm, K3: d = 2.9-3.1 mm. While the areas of bubble existence according to both analytical and TRACE models are sharp, their widening indicating inaccuracy in bubble distribution resulted from the PACO model. The difference distinctly decreases as increases the number of bubble classes being at disposal for bubble redistribution into classes of bubble sizes during calculation. A compromise is however needed as increasing number of bubble size classes considerably prolongs the calculation.

Batch bubble distribution in a model melting space

In order to verify models in a non-isothermal melting space with flowing glass, laboratory test data were used providing numbers and size distribution of bubbles coming from batch melting. Figure 15 presents the size distribution of bubbles coming from the laboratory test. The initial bubble composition was chosen as 95 vol.% CO_2 and 5 vol.% N_2. Besides the laboratory input value of bubble concentration 4.667×10^6 bubbles/m^3, the ten times higher concentration was tested too. Both bubble distribution models (TRACE and PACO) were tested. Bubbles were evenly released from the batch blanket or inputted the melt only from the front part of the blanket. The model melting space was 10 m long, 4 m wide with the glass melt layer 1 m thick. The temperature and glass velocity distributions inside the tank were calculated by using GLASS MODEL [16]. Effect of bubbles on glass temperature and velocity distribution was also considered in these calculations [17]. When evaluating bubble concentration fields in the melting space, a simple representation of this quantity is needed. The average concentrations of bubbles in cross section layers having thickness 1 m as a function of the space length were applied in this work. The mentioned representation provides an overall picture of bubble space distribution. As an example, following Figures 16 and 17 present two cases of relations between average bubble concentrations and space length. Figure 16 presents the bubble distribution for bubbles released from the front part of the batch blanket (ten times higher bubble input concentration) when using the TRACE distribution model and both simplified and complete bubble models. The bubble impact on glass flow and temperature distribution was not considered. As is obvious from the figure, the bubble concentrations according to complete model are lower compared to the simplified one. This difference is due to higher bubble growth rates in the complete model during earlier stages of bubble life (see Figures 3-5). Despite this difference, the bubble removing process is accomplished at the almost identical value of X-coordinate. The similar picture for both bubble models is provided by Figure 17 where the

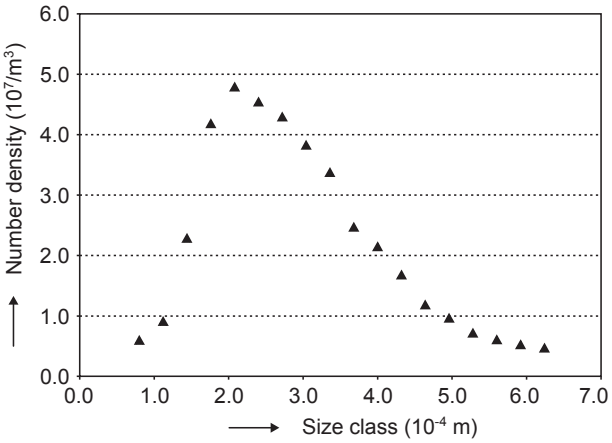

Figure 15. The size distribution of bubbles coming from the laboratory test.

impact of bubbles on the melt temperature and velocity fields was considered as well. The concentration peaks in Figure 17 are consequence of intensive melt circulation in the below batch region. Both comparisons prove that application of the simplified bubble model under real melting conditions is acceptable. The overall pictures of bubble distribution at higher bubble input concentration, as well as the temperature and the velocity distributions in the melt, are however different below the batch region giving the evidence about significant bubble impact on the melt behaviour, when the bubble concentration is high.

CONCLUSIONS

The simplified model of single bubbles neglects the initial non-stationary period of mass transfer of gases from melt, ensuing from the difference between the bubble initial and stationary composition. In addition, the simplified model assumes the stationary composition sets up instantly after temperature change. The slower setting up bubble stationary composition in a quiescent melt is characterized by slower bubble growth in the complete model under condition of temperature increase and by slower bubble dissolution if temperature sinks.

Both facts are projected into behaviour of real bubbles in a real glass melting space. When applying the real initial bubble compositions, a satisfactory agreement between the complete and simplified solutions exists for most of bubbles.

The verification of bubble distribution models shows that the model of bubble representatives exhibits very acceptable accuracy for calculation of bubble distribution in the plug flow channel and similar result can be expected for a more complicated glass flow. The accuracy of the convective model of bubble distribution improves with incerasing number of classes of bubble sizes, used for the simulation.

The calculation of bubble concentration fields in the non-isothermal melting space with glass flow showed acceptable differences between both bubble models and justified the application of the simplified model (Equations (9)-(10)) characterized by limited scope of experimental data and describing fining process always with satisfactory fidelity.

The further development of distribution models leads to their simultaneous application. The adequate experimental methods and procedures are needed to get data into refining models. The high temperature observations of bubble kinetics belong to the frequently used.

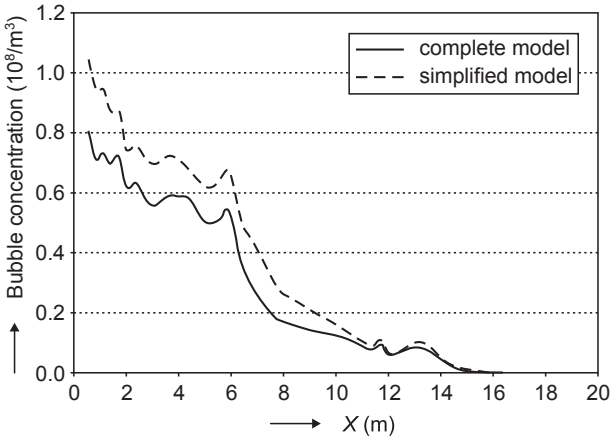

Figure 16. The average bubble concentrations released from the front part of the batch blanket vs. the model space length. The effect of bubbles on the glass flow was not considered.

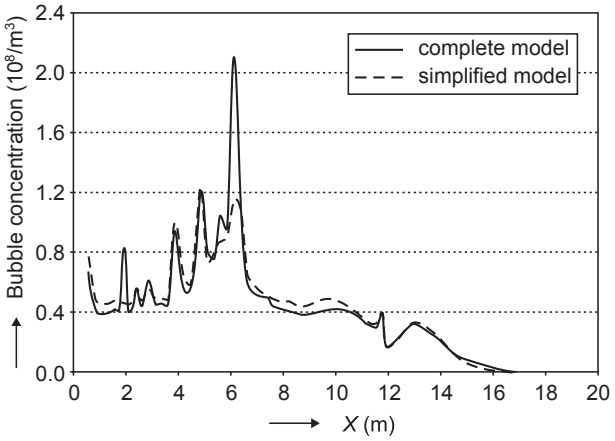

Figure 17. The average bubble concentrations released from the front part of the batch blanket vs. the model space length. The effect of bubbles on the glass flow was considered.

Acknowledgement

This work was a part of the projects No. 2A-1TP1/063, "New glass and ceramic materials and advanced concepts of their preparation and manufacturing", realized under financial support of the Ministry of Industry and Trade of the Czech Republic and the Research Programme MSM 6046137302 of the Czech Ministry of Education, Youth and Sport.

Financial support of the Schott Glass, Mainz, Germany is appreciated.

References

1. Jebavá M., Němec L., Kloužek J.: Ceramics-Silikáty *48*, 121 (2004).
2. Němec L., Kloužek J.: Ceramics-Silikáty *39*, 1 (1995).
3. Kloužek J., Arkosiová M., Němec L.: Ceramics-Silikáty *50*, 134 (2006).
4. Němec L., Jebavá M., Tonarová V.: Proceedings of the 8th International Seminar on Mathematical Modelling and Advanced Numerical Methods in Furnace Design and Operation, Velké Karlovice, Czech Republic, 2005, pp. 24-47.

5. Němec L., Jebavá M., Cincibusová P.: Ceramics-Silikáty *50*, 140 (2006).
6. Levich V.G.: *Physico-chemical Hydrodynamics*, Englewood Cliffs, New York 1962.
7. Beerkens R.C.G.: Proceedings Glass Days, Rochester, USA, 2003, pp. 1-52.
8. Ramos J.I.: J.Am.Ceram.Soc. *69*, 149 (1987).
9. Němec L., Muhlbauer M.: J.Non-Cryst.Solids *38&39*, 593 (1980).
10. Kloužek J., Němec L., Ullrich J.: Glastechn.Ber. Glass Sci.Technol. *73*, 329 (2000).
11. Kloužek J., Matyáš J., Němec L., Trochta M., Ullrich J.: Proceedings of the 5th Conference of European Glass Science and Technology, Czech Glass Society, Pratur, 199, paper No. A 2-3.
12. Kloužek J., Němec L.: Ceramics-Silikáty *47*, 155 (2003).
13. Matyáš J., Kloužek J., Němec L., Trochta M.: Proceedings of the 8th International Conference on Radioactive Waste Management and Environmetal Remediation, Bruges, Belgium, 2001.
14. Ullrich J.: PhD. Thesis, 1992, ICT, Prague.
15. Němec L., Cincibusová P.: Ceramics-Silikáty *49*, 269 (2005).
16. Schill P.: Proceedings of the 2nd International Seminar on Mathematical Modelling and Advanced Numerical Methods in Furnace Design and Operation, Vsetín - Horní Bečva, Czech Republic, 1993, pp. 102-116.
17. Matyáš J., Němec L.: Glass Sci.Technol. *76*, 71 (2003).

OVĚŘOVÁNÍ ČEŘICÍCH MODELŮ A JEJICH APLIKACE

JAROSLAV KLOUŽEK, LUBOMÍR NĚMEC, MARCELA JEBAVÁ, MIROSLAV TROCHTA*, JIŘÍ BRADA*

Laboratoř anorganických materiálů, Společné pracoviště Ústavu anorganické chemie AVČR a Vysoké školy chemicko-technologické v Praze, Technická 5, 166 28 Praha
**Glass Service, a.s., Rokytnice 60, 755 01 Vsetín*

Studie srovnává dva modely chování bublin ve sklovinách; kompletní stacionární model a zjednodušený model využívající experimentální data, tj. rychlosti růstu bublin a stacionární složení bublin. Ověření zjednodušeného modelu ve statické sklovině a v reálném tavicím prostoru ukázalo jeho přijatelnou aplikovatelnost. Dále jsou presentovány dva modely distribuce bublin v tavicím prostoru: tzv. model reprezentantů a konvektivní model. Ověřovací postup obou distribučních modelů v jednoduchém kanálu s pístovým tokem ukázal na vysokou správnost modelu reprezentantů. Podobný výsledek lze očekávat pro složitější proudění skloviny. Správnost konvektivního modelu distribuce bublin se snižuje s klesajícím počtem tříd velikosti bublin, které se použijí při výpočtu.